A first look at the atmosphere in UKESM1

Colin Jones*[1], Jane Mulcahy*[2], Stephanie Woodward*[2], Fiona O'Connor[2] and Till Kuhlbrodt*[1]

[1] National Centre for Atmospheric Science (NCAS), Met Office Hadley Centre [2].
* UKESM core group member

The core of the UKESM1 atmosphere is the GA7.1 version of the Unified Model Global Atmosphere (Walters et al. 2018, Mulcahy et al. 2018). In addition to the GA7.1 atmospheric configuration, UKESM1 also includes the UKCA stratosphere-troposphere interactive chemistry scheme, which predicts a number of key atmospheric greenhouse gases (e.g. ozone (O_3), methane (CH_4) and nitrous oxide(N_2O)), as well as the chemical oxidants that lead to the formation of atmospheric aerosol (for example the oxidation of SO_2 to SO_4^{2-} and subsequent formation of H_2SO_4). Furthermore, a number of atmospheric phenomena, which use time-invariant prescribed emission files in the physical model HadGEM3-GC3.1 (GC31 here after) are interactively coupled to other components of UKESM1. This allows for a more complete representation of the full Earth system, in particular allowing the possibility of future feedbacks across components of the Earth system. Such couplings include; (i) marine emissions of dimethlysulfide (DMS) and Primary Marine Organic Aerosol (PMOA) from time evolving fields simulated in the MEDUSA marine biogeochemistry model, (ii) terrestrial emission of Biogenic Volatile Organic Compounds (BVOCs) into the atmosphere are from the time evolving vegetation predicted by the JULES-TRIFFID land surface-vegetation scheme. Similarly, dust emissions into the atmosphere are coupled to the JULES-TRIFFID predicted land surface. Atmospheric dust is also deposited into the ocean, acting as a source of soluble iron for ocean biogeochemistry. Finally, when run in CO_2-emission mode, a full global carbon cycle is activated, with exchanges of CO_2 between the land, ocean and atmospheric components of the model.

In this article we present some initial results from a few important components of the UKESM1 atmosphere, touching on; top of atmosphere (TOA) radiation fluxes, aerosol radiative forcing, the treatment of natural marine aerosols, the representation of mineral dust and some initial results from the prognostic chemistry in UKESM1. A more detailed analysis of UKESM1 performance, both coupled and component models, will appear in the peer reviewed literature. The underpinning coupled physical model of UKESM1 (GC31 at N96 (atmosphere) and 1° (ocean) resolution) has been documented in Kuhlbrodt et al. (2018), while the GA7.1 atmospheric model configuration of GC3.1 and UKESM1 is detailed in Mulcahy et al. (2018).

1. Top of atmosphere radiation fluxes

In the introductory article to this newsletter, we showed that the global mean TOA net radiation balance in UKESM1 is essentially zero when averaged over a sufficiently long time-period. The top panel in figure 1 again shows the UKESM1 piControl TOA net radiation (in black), also shown is the GC31 TOA radiation budget (in red), which is slightly positive at around +0.2Wm^{-2}. The second and third panels in figure 1 show the piControl TOA radiation balance averaged over the northern (NH) and southern (SH) hemispheres separately, while the bottom panel shows the North minus South gradient in TOA net radiation. GC31 receives ~1Wm^{-2} more energy at the TOA in the SH compared to UKESM1 and as a consequence emits more

radiant energy back to space from the NH. As a result, the south to north net TOA meridional energy gradient is ~1.5Wm^{-2} larger in GC31 than in UKESM1. Recent studies emphasize the importance of the hemispheric gradient of TOA radiation for key aspects of the climate system such as; the location of the Inter Tropical Convergence Zone (ITCZ, Hwang and Frierson 2013) and the strength of the meridional ocean heat transport associated with the Atlantic Meridional Overturning Circulation (AMOC, Marshall et al. 2013).

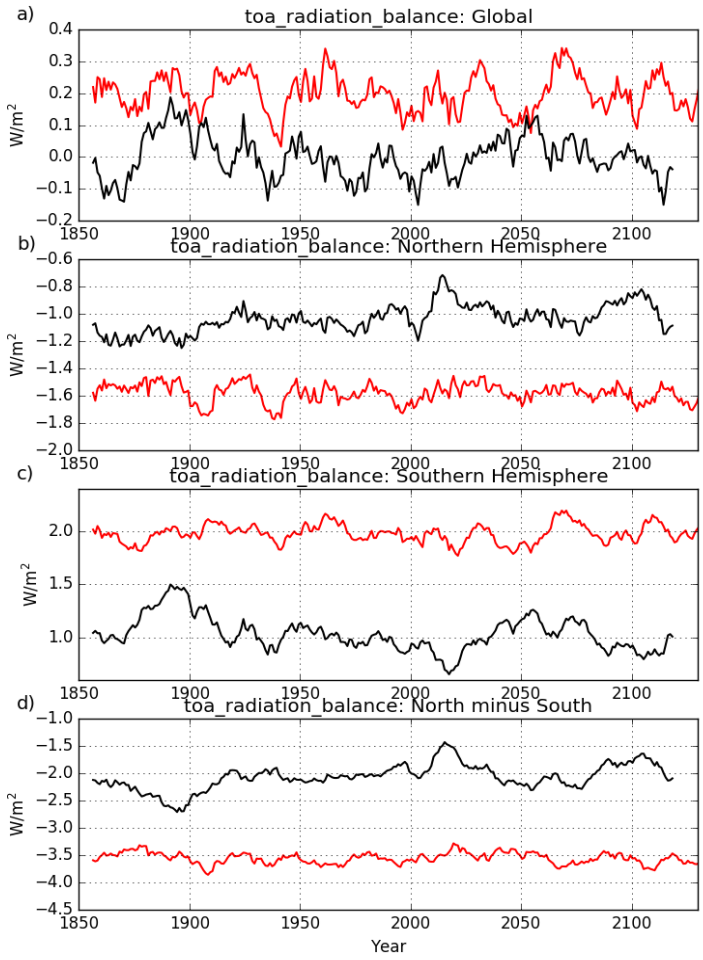

Figure 1 Top: Global mean TOA net radiation, 2nd row: Northern Hemisphere (NH) mean net TOA radiation, 3rd row: Southern Hemisphere (SH) mean net TOA radiation, bottom row: NH minus SH gradient in net TOA radiation. Results are from the UKESM piControl (black) and GC31 piControl (red). Annual values have had an 11 year running mean passed through them.

Figure 2 shows the components of the TOA radiation budget, on the left net shortwave radiation (positive values indicate radiation into the atmosphere) and on the right outgoing longwave radiation (negative values indicate energy leaving the atmosphere). The UKESM1 global atmosphere receives slightly less (~0.5Wm^{-2}) solar energy than GC31. This is equivalent to UKESM1 being is slightly more reflective than GC31 in the global mean. The main difference in reflectivity is seen in the SH, where UKESM1 is ~1.5Wm^{-2} more reflective (receives less net solar energy at TOA) than GC31. The bulk of this difference is in the latitude band ~35°S to 70°S and is associated with a slight increase in cloud fraction and, more importantly for total reflectivity, clouds that are brighter due to having more cloud droplets that

are smaller in mean radius than GC31. This change comes about from (i) including marine PMOA emissions from the ocean into the UKESM1 atmosphere and (ii) linking both the surface flux of PMOA and DMS to the MEDUSA ocean biogeochemistry model. Both these changes lead to more natural aerosol emitted into the UKESM1 atmosphere over the southern ocean and a greater number of cloud droplets are activated. As GC31 is known to have a negative bias in total sky reflectivity for present-day conditions, we consider an increase in reflectivity in UKESM1 relative to GC31 as a performance improvement.

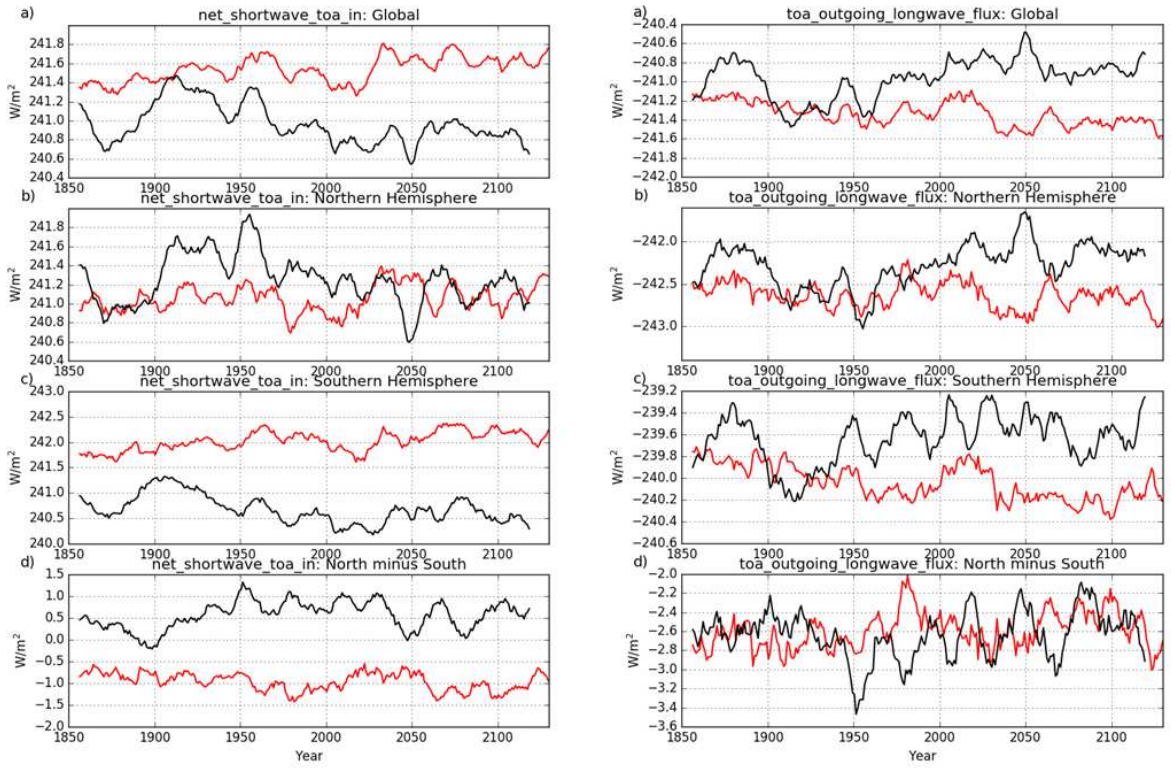

Figure 2: As figure 1 but left panel is net shortwave radiation at TOA and right panel is OLR.

The bottom left panel in figure 2 shows the meridional (NH minus SH) gradient in TOA net solar radiation. UKESM1 has slightly more net solar energy entering the NH than SH, by ~0.5Wm^{-2}, indicating that the SH is more reflective than the NH. GC31 has the converse, with the SH receiving ~1Wm^{-2} more net solar energy than the NH. As these runs are for pre-industrial (PI) conditions it is difficult to apply an observational constraint. Nevertheless, satellite observations (Stephens et al. 2016) for the present-day (PD, ~2000 -2014 period) indicate that the SH and NH receive approximately the same amount of net solar radiation (i.e. an NH minus SH gradient of zero). The primary (although not only) difference in total solar reflectivity going from a PD to a PI climate is the loss of anthropogenic aerosols. These are relatively short-lived species, which primarily influence the northern hemisphere, causing an increase in the PD total sky reflectivity relative to PI conditions. Therefore, going from PD to PI one should expect the real world total reflectivity to decrease as anthropogenic aerosols disappear, with this decrease being primarily in the NH. This implies, if there had been observations of TOA net solar radiation in the pre-industrial period they would likely have seen a planet with a more reflective SH than NH (i.e. the net NH minus SH gradient in TOA solar radiation would have been positive). This thought experiment, combined with the PD

observations and the known southern hemisphere PD biases in GC31, taken together, suggest the UKESM1 TOA net solar radiation field is likely more realistic than GC31.

The right panel of figure 2 shows the TOA outgoing longwave radiation (OLR). Due to the lower amount of incoming solar radiation, the UKESM1 climate system is slightly colder than GC31, which is evident in the lower OLR values in UKESM1 (~0.4Wm^{-2} less than GC31), which is primarily a decrease in the SH OLR. Generally, we believe the UKESM1 piControl TOA radiation budget is slightly more accurate than GC31 in terms of hemispheric structure, although this contention will need to be more thoroughly tested against observations in the latter period of the CMIP6 historical simulations.

2. Aerosol Effective Radiative Forcing and natural aerosols

Mulcahy et al (2018) document the suite of model improvements that took the UM Global Atmosphere configuration (GA7.0) and coupled configuration (GC3.0) to respectively, GA7.1/GC3.1, which constitute the physical model core of UKESM1. These developments were necessary to remedy an excessively large negative aerosol effective radiative forcing (ERF) over the historical period in GA7.0/GC3.0, which was diagnosed to be -2.75Wm^{-2} for year 2000 minus 1850 emissions. Such a large and negative forcing is well outside the IPCC AR5 best estimate and would lead to an historical total radiative forcing close to zero, at odds with the observed warming over the historical past. Figure 3 shows the total historical aerosol ERF from GA7.0 (left column) and GA7.1 (right column). The top row shows the total aerosol ERF, the second row the direct (clear sky) ERF and the bottom the ERF due to both the direct effect and the 1st cloud (indirect) effect (the Twomey effect from increasing cloud droplet number and albedo as aerosol number increases at a fixed liquid water amount). The primary cause of the reduction in aerosol ERF from GA7.0 to GA7.1 is the large decrease in the 1st indirect effect, primarily due to an improved treatment of cloud droplet spectral dispersion in the calculation of droplet effective radius (see Mulcahy et al. 2018). The aerosol direct ERF also decreases, due to a more accurate treatment of black carbon aerosol optical properties. Combined with other components of the total historical radiative forcing (e.g. historical emissions of CO_2, O_3, CH_4 and N_2O and human land use changes) the total historical UKESM1 ERF for year 2000 minus 1850, using CMIP6 emissions is +1.77Wm^{-2}.

A key component of accurately simulating the historical aerosol radiative forcing lies in representing natural aerosols, which define the pre-industrial aerosol climate. In UKESM1, over the ocean, we interactively simulate marine emissions of DMS and Primary Marine Organic Aerosol (PMOA). DMS is oxidized in the atmosphere to form sulfate particles and is known to have a significant impact on cloud droplet number (Kruger and Grassl 2012). DMS and PMOA emissions are associated with biological activity in the ocean (O'Dowd et al. 2004). Hence, to allow for potential future feedbacks involving climate, ocean biology and aerosol emissions, we link the emission of both species to simulated ocean biology from MEDUSA, following the parameterizations of Anderson et al. (2001), for DMS and Gantt et al. (2012) for PMOA. GC31 does not include a formal parameterization of PMOA emissions, to account for this omission in GC31 DMS emissions were multiplied by a factor of1.7. Furthermore, DMS emissions in GC31 are parameterized using an observation-based seawater DMS climatology (Lana et al. 2011). While this provides relative accuracy for present-day conditions, it

precludes the possibility of simulating future changes in ocean biology and their impacts on DMS or PMOA.

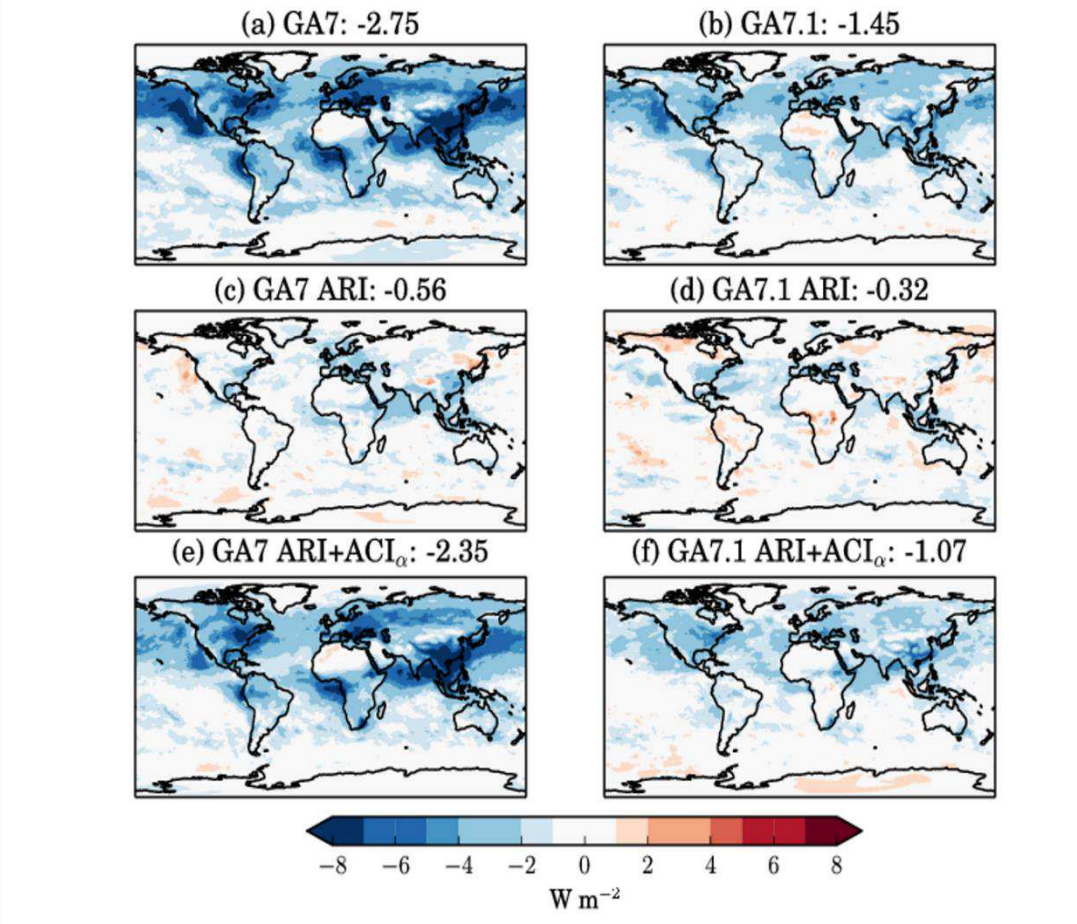

Figure 3. Total historical aerosol ERF (top), direct aerosol ERF (middle) and direct + 1st indirect effect (bottom). GA7.0 is on the left and GA7.1 (atmospheric component of UKESM1) the right.

Figure 4 illustrates the annual cycle of seawater DMS (right) and organic mass concentration (of PMOA, left) simulated by UKESM1. The mean annual cycle of seawater DMS is an average over the Southern Ocean (40°S-65°S) plotted for from UKESM1 (red) and the Lana observations (black). The black vertical lines represent inter-annual variation in the monthly Lana values and the red lines the same statistic from UKESM1. The well-known annual cycle in surface DMS is visible, with maximum values in the austral summer. UKESM1 captures the annual distribution quite well, although the amplitude of the annual cycle is somewhat weaker than observed. The organic mass concentration of marine aerosol (left panel) simulated by UKESM1, (dashed red line) is compared to observations from Amsterdam Island in the Southern Ocean. Again, a clear annual cycle is visible in the observed organic mass concentration, associated with ocean biological activity. This cycle is also well captured by UKESM1, suggesting an interactive treatment of both DMS and PMOA emissions do not degrade the treatment of natural aerosol in the model. In fact, the improved (increased) shortwave reflectivity in UKESM1, compared to GC31, over the Southern Ocean (shown in figure 2) largely arises because of the inclusion of the PMOA emission parameterization in UKESM1 and the linking of both PMOA and DMS emissions to the UKESM1 ocean biology.

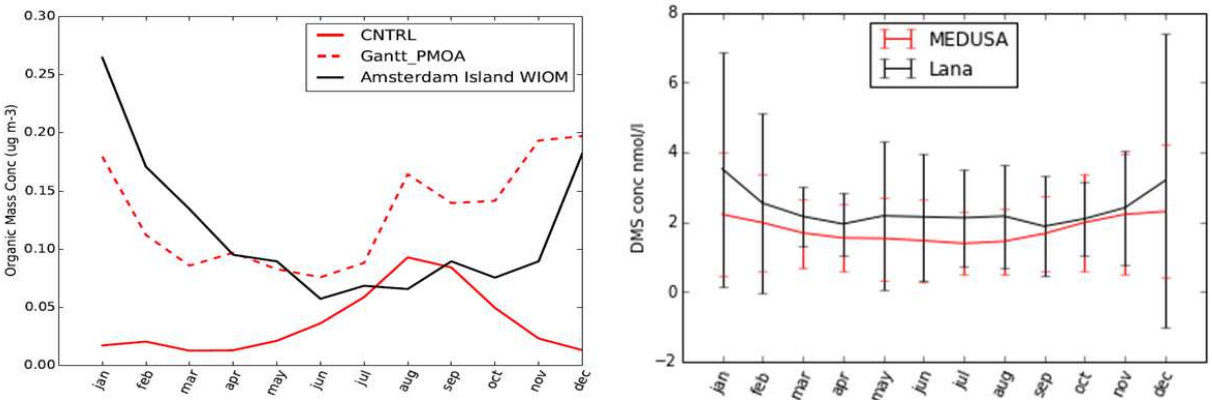

Figure 4: Left panel; Mean annual cycle of organic mass concentration of aerosol particles at the ocean surface observed at Amsterdam Island (black) and simulated for the same grid box location in UKESM1 (red dashed line). Right panel; Southern ocean (40°S-65°S) mean annual cycle of seawater DMS from Lana observations (black) and UKESM1 (red).

In figure 5 we illustrate the importance of natural marine aerosol for the cloud droplet number concentration (CDNC) over the Southern Ocean. For a given cloud liquid water amount, the greater the aerosol number, the greater the number of (smaller) cloud droplets, leading to an increased cloud albedo. The black full line in figure 5 is an estimate of mean annual cycle of CDNC, at 1km altitude, derived from the MODIS satellite instrument. A peak in CDNC is seen in the austral summer (November to February), coincident with maximum surface marine biological activity. The black dashed line in figure 5 (labelled DMSx0) is when the UKESM1 atmosphere is run with only sea-salt emissions active (i.e. non marine biological contribution to aerosol emission). This can be considered as the “background” CDNC over the Southern Ocean. Inclusion of DMS emission, linked to the Lana DMS climatology (labelled DMSx1.0) results in the red dashed line, with a weak summer season maximum in CDNC. The full and dashed blue lines represent maximum and minimum values of CDNC based on the extremes of the quoted uncertainty ranges in the Lana climatology. In GC31 we account for the lack of PMOA emissions by scaling the simulated DMS emissions by x1.7 (Mulcahy et al. 2018), this results in the red full line, with a large annual cycle of CDNC, closer to the observed estimates. Finally, in light blue are two UKESM1 atmosphere simulations where the 1.7 scaling on DMS has been removed and the Gantt et al. (2012) PMOA emission parameterization included. The two lines differ in the scaling applied to the organic mass fraction assumed to be associated with sea salt in the Gantt scheme. Clearly, the amplitude of the CDNC annual cycle increases after addition of the PMOA emission scheme, bringing the summer season CDNC close to the MODIS observations.

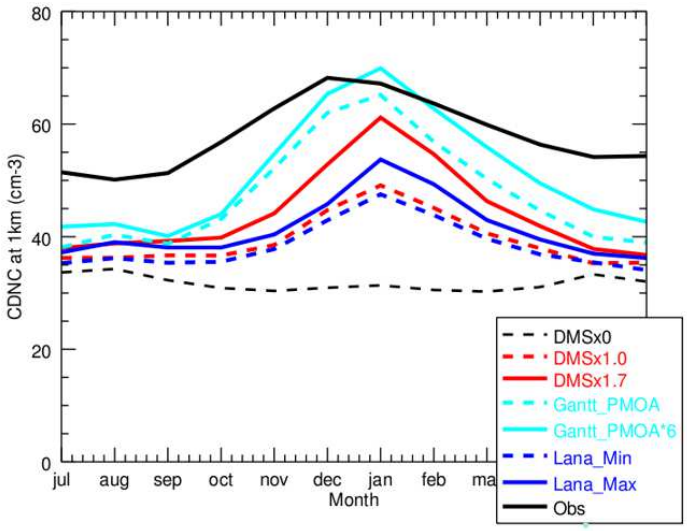

Figure 5. Mean annual cycle of cloud droplet number concentration (CDNC) over the Southern ocean, derived from MODIS observations (full black line) and from various configuration of the UKESM1 atmosphere (see text for details).

3. Mineral dust in UKESM1

The representation of mineral dust in UKESM1 is based on the same well-tested scheme used in HadGEM3 (Johnson et al. 2016) and the predecessor UK Earth system model used in CMIP5; HadGEM2-ES (Woodward, 2011). Minimal changes were introduced to UKESM1 compared to the current HadGEM3-GC3.1 configuration. These include; 1) Dust emission from seasonal sources in vegetated areas was switched off, as its inclusion increases the dependence of dust on the interactively simulated vegetation, which had been seen to cause problems in earlier work with HadGEM2-ES; and 2) the dust scheme was retuned for the new model, with the 3 tuneable parameters adjusted empirically to provide the best agreement with observations of dust concentrations, AODs, deposition rates and size distributions. Some tuning of the vegetation scheme was also performed, which improved the representation of bare soil fraction and hence dust source areas. Through this approach, an acceptable dust simulation was achieved without the need for preferential source areas to limit emissions, as required in many models.

A comparison of near-surface dust concentrations and AODs from a UKESM1 historical run (1990-2009) with observations from the University of Miami network and AERONET is shown in figure 6, together with the equivalents from the coupled GC31 and the earlier ESM HadGEM2-ES. In UKESM1 Atlantic dust concentrations are well-simulated, whilst in the Pacific concentration are very slightly high and in the Southern Ocean low. AODs in the Sahel are also slightly low. Overall, however, the agreement with observations is good – certainly considerably better than HadGEM2-ES, and comparable to GC31. This improvement from the earlier model is largely due to improved ESM performance, most directly in the simulation of bare soil fraction. The dust scheme in each model the same apart from the use of preferential source areas in HadGEM2-ES, seasonal sources in GC31, and individual tuning for each.

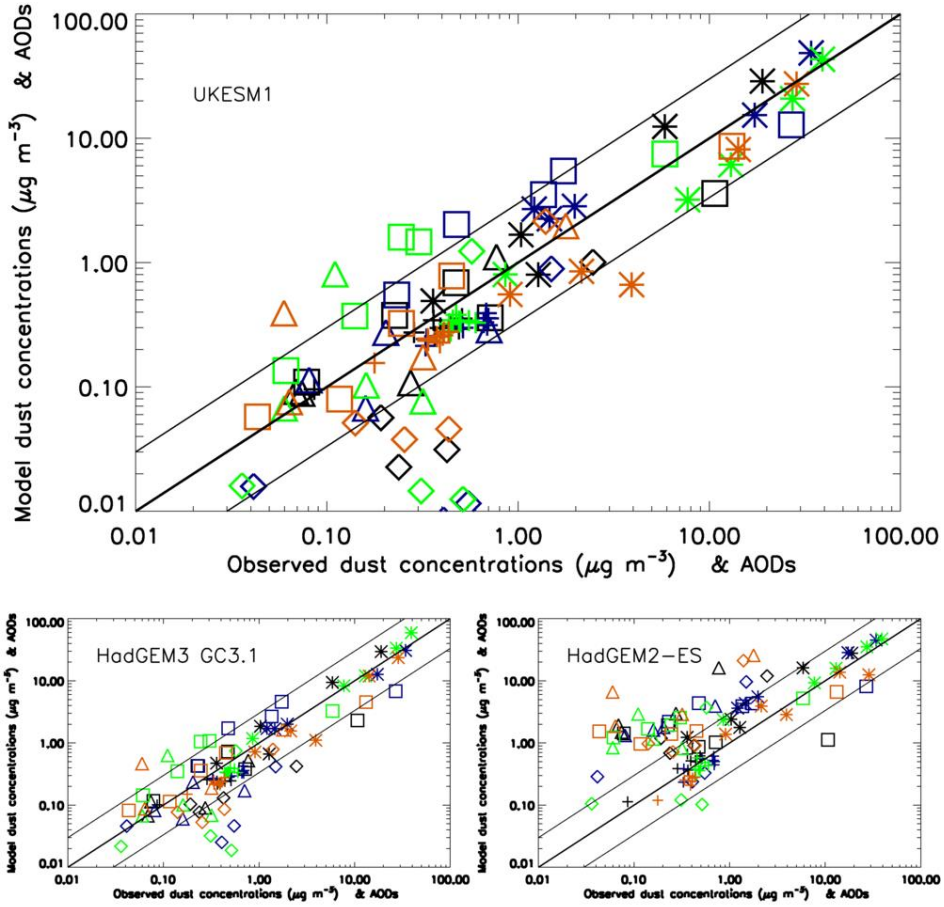

Figure 6. Seasonal mean near-surface dust concentrations and AODs from 20 years of UKESM1 (1990-2009), HadGEM3-GC3.1 (1990-2009) and HadGEM2-ES (1985-2004 - later data not available) plotted versus observations. Concentration data from University of Miami stations in the Atlantic (stars), N Pacific (squares), S Pacific (triangles) and Southern Ocean (diamonds), and AOD data from dust-dominated AERONET stations, mostly in the Sahel (crosses). Colours indicate seasons (djf black, mam blue, jja green, son red).

Tuning of the dust size distribution against observations was introduced for the first time in UKESM1. Normalised volume size distributions for the appropriate location and season were compared with data from the FENNEC campaign of June 2011 (Ryder et al. 2013), chosen as it included flights close to dust sources and measured a wide range of particle sizes, including very coarse sizes. Though dust concentrations and AODs were the primary tuning reference, where two or more combinations of settings gave similar performance against these data, the one which produced the better size distribution was chosen. Figure 7 shows that the size distribution from a UKESM1 historical simulation agrees well with observations across almost the whole modelled range, and is very close to the observational mean for the 4 central size bins. In UKESM1 the concentration of the largest particles in the 20-63 micron diameter bin is just below the mean from the observations, possibly due to the difference between model monthly means and observations taken preferentially during dusty periods, as local dust events give higher concentrations of the largest particles which fall out of the atmosphere very rapidly. The cause of the small low bias of the finest particles is not yet clear: it may be due to a bias in emission size distribution or to underestimated emission flux remotely from the measurement area. Comparison of a climatological mean from the model with data from a

single measurement campaign is not expected to be exact, though it is still indicative and useful in the absence of long-term measurements of such size distributions.

The results of this initial assessment of dust in UKESM1 are encouraging, particularly the level of agreement with observations given that the dust scheme is driven by an earth system model, where the additional processes and feedbacks inevitably complicate the simulation of fields such as bare soil, wind-speed and soil moisture, on which dust emissions strongly depend. A realistic simulated size distribution will help deliver a good simulation of the size-dependent dust processes including, most importantly, the radiative impact. With the assessment of present-day performance complete, the dust simulation within UKESM1 will be used, both to investigate the behaviour of the mineral dust itself and to assess its impact on climate through radiative and biogeochemical mechanisms within the full earth system.

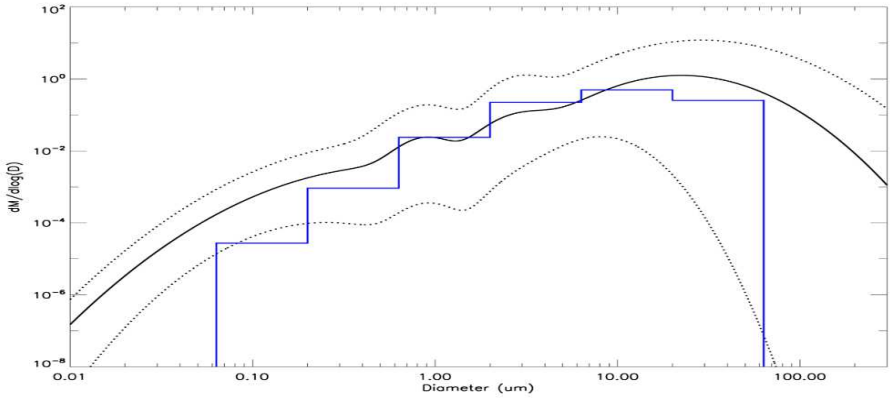

Figure 7. Normalised dust mass size distributions from UKESM1 historical run and lognormal fit to minimum, maximum and mean of FENNEC data (Ryder, 2013). UKESM data is the mean of 20 Junes (1990-2009), from NW Sahara (12-6W, 21-26N), level 2 (approx 50m).

4. Trace gas atmospheric chemistry in UKESM1

Gas-phase chemistry in UKESM1, is modelled interactively using the United Kingdom Chemistry and Aerosol (UKCA; *http//:www.ukca.ac.uk*) model. UKCA simulates gas-phase chemistry throughout the depth of the atmosphere, combining the stratospheric chemistry from Morgenstern et al. (2009) with the tropospheric "TropIsop" chemistry scheme from O'Connor et al. (2014). Photolysis rates are calculated interactively using Fast-JX (Neu et al. 2007; Telford et al. 2013) and respond to changes in surface albedo, cloud amounts, and overhead ozone column. Further advances in the treatment of gas-phase chemistry and its interactions with other Earth System components in UKESM1 include:

(i) Interactive terrestrial emissions of isoprene and monoterpenes (Pacifico et al. 2011).
(ii) Production of secondary organic aerosol precursors (Kelly et al. 2018) for the aerosol component of UKCA; GLOMAP-mode (Mann et al. 2010; Mulcahy et al. 2018).
(iii) Feedbacks onto radiation from whole-atmosphere methane, ozone, nitrous oxide, as well as water vapour from methane oxidation in the stratosphere and lower mesosphere.

Here we present two examples of simulated ozone from one of the UKESM1 historical experiments, comparing the period 2000-2010 from this run against available observations. Figure 8 compares regionally aggregated tropospheric ozone on different pressure levels

against ozone observations. Figure 9 compares vertically resolved ozone against a new observational data set (Bodeker et al. 2013), plotted as a function of latitude and height and as a scatter plot (model against observations) for different latitude bands.

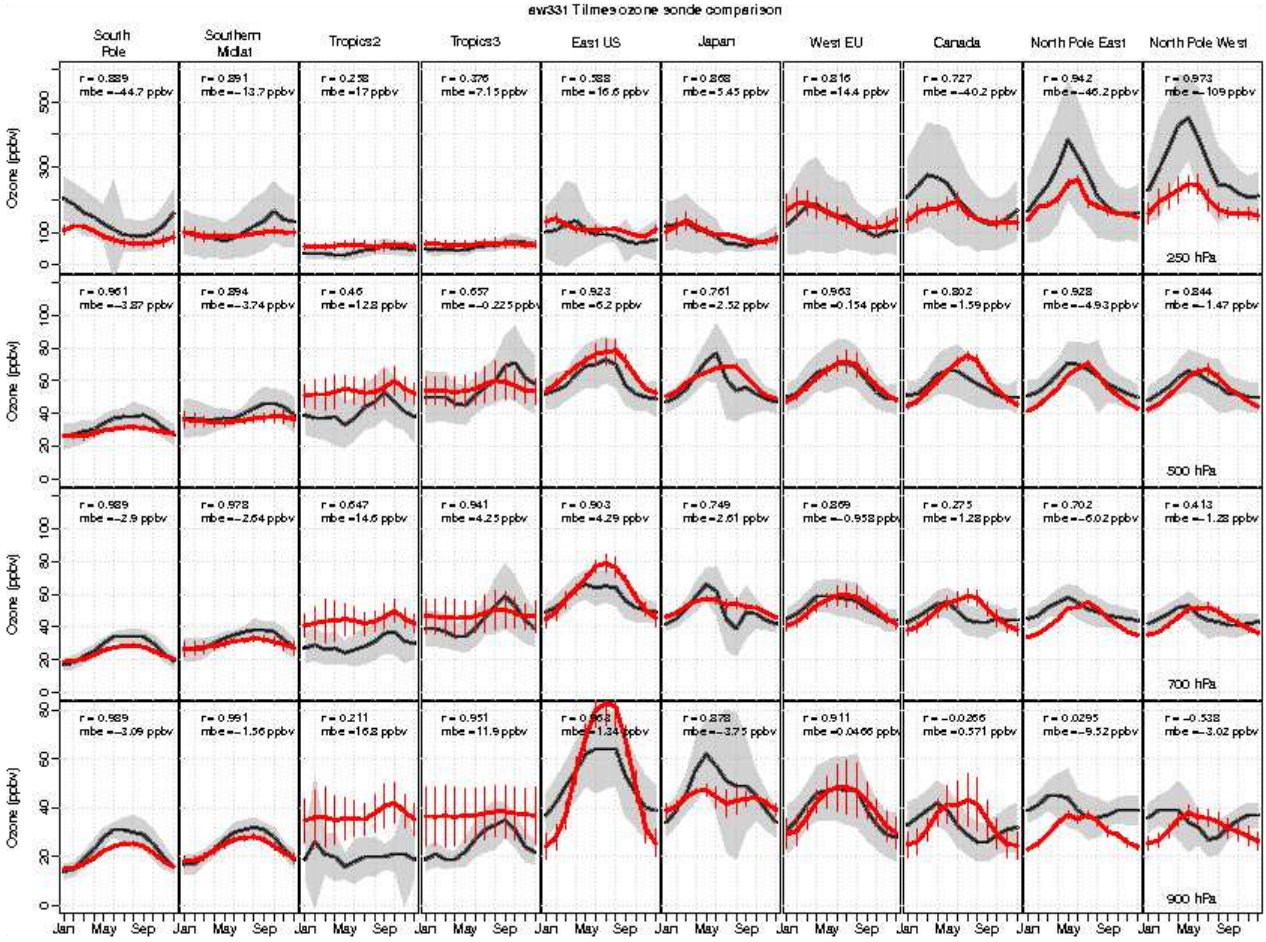

Figure 8: Comparison of the seasonal cycle in modelled ozone for 2000-2010 from one UKESM1 historical simulation against the observational dataset of Tilmes et al., 2012

While there are some discrepancies, on the while both tropospheric and stratospheric ozone appears to be well simulated in UKESM1. The new capability for full atmosphere coupled climate-chemistry interaction provided by UKESM1 represents an excellent tool for community-wide composition-climate studies.

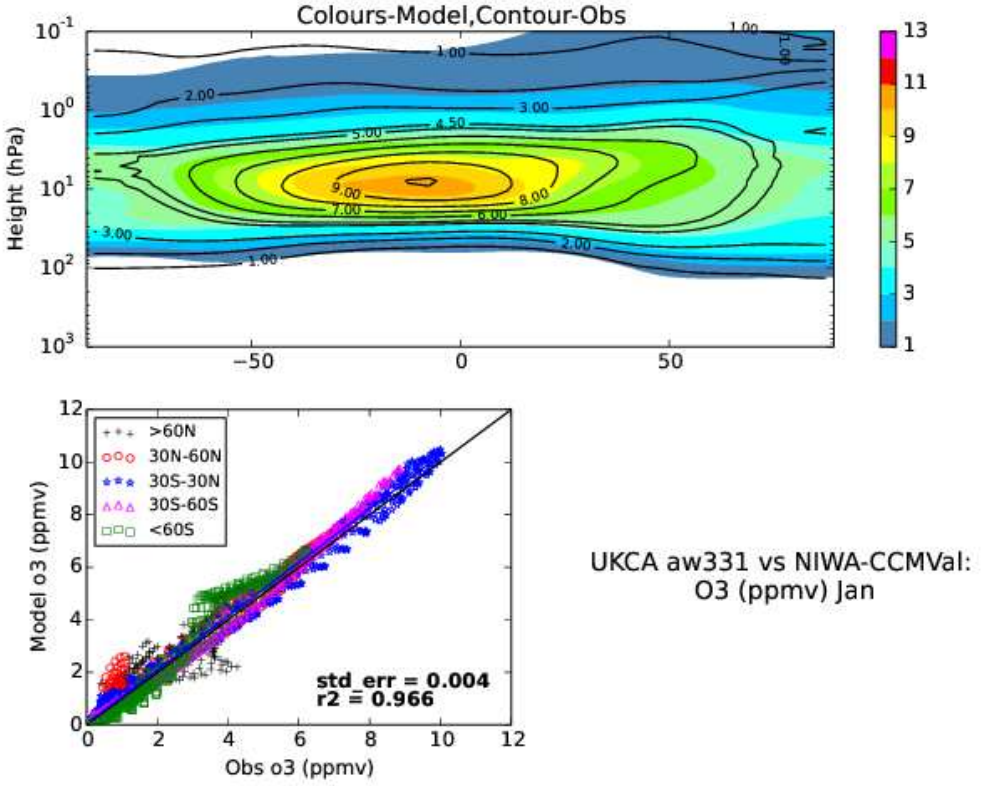

Figure 9: Comparison of vertically resolved modelled ozone in January for 2000-2010 from one of the UKESM1 historical transient simulations against a climatological observational dataset (Bodeker et al., 2013).

REFERENCES

- Anderson, T.R.; Spall, S.A.; Yool, A.; Cipollini, P.; Challenor, P.G.; Fasham, M.J.R.. 2001 Global fields of sea surface dimethylsulfide predicted from chlorophyll, nutrients and light. *Journal of Marine Systems*, 30 (1-2). 1-20.10.1016/S0924-7963(01)00028-8.
- Bodeker G.E, B. Hassler, P. J. Young, and R. W. Portmann, A vertically resolved, global, gap-free ozone database for assessing or constraining global climate model simulations, *Earth Syst. Sci. Data*, 5, 31–43, http://www.earth-syst-sci-data.net/5/31/2013/, 2013.
- Gantt, B., Johnson, M. S., Meskhidze, N., Sciare, J., Ovadnevaite, J., Ceburnis, D., and O'Dowd, C. D.: Model evaluation of marine primary organic aerosol emission schemes, *Atmos. Chem. Phys.*, 12, 8553-8566, https://doi.org/10.5194/acp-12-8553-2012, 2012.
- Hwang, Y.-T., and D. M. W. Frierson, 2013: Link between the double-intertropical convergence zone problem and cloud biases over the Southern Ocean. *Proc. Natl. Acad. Sci. USA*, 110, 4935–4940, doi:10.1073/pnas.1213302110.
- Johnson C.E. et al. (2016) Unified Model Documentation Paper 020 - CLASSIC Aerosol Scheme
- Kelly, J. R. Doherty, F. M. O'Connor, and G.W. Mann, The impact of biogenic, anthropogenic, and biomass burning emissions on regional and seasonal variations in secondary organic aerosol concentrations, *Atmos. Chem. Phys.*, 2018.
- Krüger, O., and H. Graßl (2011), Southern Ocean phytoplankton increases cloud albedo and reduces precipitation, *Geophys. Res. Lett.*, 38, L08809, doi: 10.1029/2011GL047116.
- Kuhlbrodt T**,** C. G. Jones, A. Sellar, D. Storkey, E. Blockley, M. Stringer, R. Hill, T. Graham, J. Ridley, A. Blaker, D. Calvert, D. Copsey, R. Ellis, H. Hewitt, P. Hyder, S. Ineson, J. Mulcahy, A. Siahaan and J. Walton (2018): The low-resolution version of HadGEM3 GC3.1: Development and evaluation for global climate. *Journal of Advances in Modeling Earth Systems, in review.*

- Lana, A., et al. (2011), An updated climatology of surface dimethlysulfide concentrations and emission fluxes in the global ocean, *Global Biogeochem. Cycles*, 25, GB1004, doi: 10.1029/2010GB003850.
- Mann, G. W., Carslaw, K. S., Spracklen, D. V., Ridley, D. A., Manktelow, P. T., Chipperfield, M. P., Pickering, S. J., and Johnson, C. E.: Description and evaluation of GLOMAP-mode: a modal global aerosol microphysics model for the UKCA composition-climate model, *Geosci. Model Dev*., 3, 519–551, doi:10.5194/gmd-3-519-2010, 2010.
- Marshall, J., A. Donohoe, D. Ferreira, and D. McGee (2013), The ocean's role in setting the mean position of the Inter-Tropical Convergence Zone*, Climate Dynamics*, 42(7-8), 1967-1979, doi:10.1007/s00382-013-1767-z.
- Morgenstern, O., P. Braesicke, F.M. O'Connor, A.C. Bushell, C.E. Johnson, and J.A. Pyle, Evaluation of the new UKCA climate-composition model. Part I. The stratosphere, *Geosci. Model Dev*., 2, 43-57, 2009.
- Mulcahy et al., Improving aerosol processes and effective radiative forcing in HadGEM3 and UKESM1, J. *Adv. Model. Earth System*, In preparation, 2018.
- Neu, J., Prather, M., and Penner, J.: Global atmospheric chemistry: integrating over fractional cloud cover, *J. Geophys. Res.,* 112, D11306, 12 pp., doi:10.1029/2006JD008007, 2007.
- O'Connor, F. M., C.E. Johnson, O. Morgenstern, N.L. Abraham, P. Braesicke, M. Dalvi, G.A. Folberth, M.G. Sanderson, P.J. Telford, A. Voulgarakis, P.J. Young, G. Zeng, W.J. Collins, and J.A. Pyle, Evaluation of the new UKCA climate-composition model. Part II. The troposphere, *Geosci. Model Dev*., 7, 41-91, 2014.
- O'Dowd C et al 2004. Biogenically driven organic contribution to marine aerosol. Nature 431, 676-680
- Pacifico, F., S. P. Harrison, C. D. Jones, A. Arneth, S. Sitch, G. P. Weedon, M. P. Barkley, P. I. Palmer, D. Serca, M. Potosnak, T.-M. Fu, A. Goldstein, J. Bai, and G. Schurgers¸ Evaluation of a photosynthesis-based biogenic isoprene emission scheme in JULES and simulation of isoprene emissions under present-day climate conditions, *Atmos. Chem. Phys*., 11, 4371–4389, doi:10.5194/acp-11-4371-2011, 2011.
- Ryder, C.L. et al. (2013) Optical properties of Saharan dust aerosol and contribution from the coarse mode as measured during the Fennec 2011 aircraft campaign. *Atmos. Chem. Phys*., 13, 303–325.
- Stephens, G.L., Hakuba, M.Z., Hawcroft, M. et al. *Curr Clim Change Rep* (2016) 2: 135. https://doi.org/10.1007/s40641-016-0043-9
- Telford, P. J., N.L. Abraham, A.T. Archibald, P. Braesicke, M. Dalvi, O. Morgenstern, F. M. O'Connor, N. Richards, and J.A. Pyle, Implementation of the Fast-JX Photolysis scheme into the UKCA component of the MetUM chemistry climate model, *Geosci. Model Dev*., 6, 161-177, 2013.
- Tilmes, S., J.-F. Lamarque, L. K. Emmons, A. Conley, M. G. Schultz, M. Saunois, V. Thouret, A. M. Thompson, S. J. Oltmans, B. Johnson, and D. Tarasick, Technical Note: Ozonesonde climatology between 1995 and 2011: description, evaluation and applications, *Atmos. Chem. Phys*., 12, 7475–7497, www.atmos-chem-phys.net/12/7475/2012/, doi:10.5194/acp-12-7475-2012, 2012
- Woodward S. (2011) Hadley Centre Technical Note 87 - Mineral Dust in HadGEM2 https://www.metoffice.gov.uk/binaries/content/assets/mohippo/pdf/l/p/hctn_87.pdf